Dynamics of liquid crystal vortex in a layered superconductor

Hiroyoshi Nobukane,[1,2] Erika Uno,[1] Yuichi Tabata,[1] Kyosuke Takahashi,[1] Daiki Sakabe,[3] and Satoshi Tanda[2,3]
[1]*Department of Physics, Hokkaido University, Sapporo 060-0810, Japan*
[2]*Center of Education and Research for Topological Science and Technology, Hokkaido University, Sapporo 060-8628, Japan*
[3]*Department of Applied Physics, Hokkaido University, Sapporo 060-8628, Japan*

(Received 12 December 2023; revised 28 March 2024; accepted 11 April 2024; published 2 May 2024)

We report the dynamics of liquid crystal vortices in layered dilute Fe-doped NbS_2 superconductors. We observed enhanced superconductivity with Fe atom doping. The thermally activated vortex flow causes a broad resistive transition. The temperature dependence of the melting field H_m on the applied magnetic field exhibits an upturn behavior as the temperature decreases. The result indicates that the vortex has transitioned from solid to liquid crystal phase. The in-plane anisotropy with twofold symmetry results from the different number of vortex pairs that stably exist on conduction planes when liquid crystal vortices move between neighboring layers. We suggest that under high magnetic fields, the resistance is suppressed due to the pinning of three-dimensional vortices formed by aligned vortex loops.

DOI: 10.1103/PhysRevB.109.174505

I. INTRODUCTION

Topological objects such as solitons, vortex lines, and domain walls play an important role in determining the physical properties in condensed matter physics and various other systems [1,2]. These are mathematically classified into homotopy classes according to order parameter and dimensionality. In particular, a quantized vortex is a topological defect in superconductors and superfluids characterized by a geometric phase with an integer number. As a topological excitation in two dimensions, a metastable long-range order emerges by generating vortex-antivortex pairs [3,4]. The intermediate state of strongly anisotropic superconductors exhibits a variety of vortex phases similar to liquid crystals due to the pancake vortices found in planes and Josephson vortices confined between layers [5–8]. The fractional quantum Hall effect has been predicted in vortex liquids consisting of boson systems [9]. These studies have performed well in cuprate superconductors [10–12]. However, a high magnetic field is required to investigate multiple vortex solid-liquid phases. Therefore, we have studied liquid-crystal-like vortex states in anisotropic transition metal dichalcogenides (MX_2, where M is a group-4 or -5 metal and X = S, Se, or Te). We can detect vortex interactions and dynamics in MX_2 superconductors through electric transport measurements.

With 2H-MX_2, there is a competitive or coexisting relationship between superconductivity and a charge density wave (CDW). The coexistence of CDW and pair density wave states was recently discovered in 2H-$NbSe_2$ [13]. One of the MX_2 materials, 2H-NbS_2, exhibits superconductivity at 5 K without showing a CDW at higher temperatures and shows stronger anisotropy than 2H-$NbSe_2$ [14]. It has been pointed out that 2H-NbS_2 exhibits a Fulde-Ferrell-Larkin-Ovchinnikov (FFLO) state at low temperatures and high magnetic fields [15]. Moreover, theoretically, a unique superconducting mechanism in NbS_2 has been pointed out [16]. To clarify unusual electronic states, we have studied the physical properties of Fe-doped NbS_2 [17]. By doping Fe atoms, the interlayer distance increases so that the two dimensionality can be enhanced. Recent scanning tunneling microscopy (STM) measurements reveal the coupling between vortices and Yu-Shiba-Rusinov (YSR) states at the magnetic impurities [18]. Thus, we can reveal exotic vortex states in Fe-doped NbS_2. In addition, there is the possibility that CDW order can be induced.

In this paper, we report the dynamics of liquid crystal vortices in layered dilute Fe-doped NbS_2 superconductors. The enhancement of H_{c2} and T_c was observed. Fe-doped NbS_2 shows a broad superconducting transition due to vortex flow. The temperature dependence of the vortex melting magnetic field H_m displays an upward turn as the temperature decreases. The result suggests a transition to a liquid-crystalline-like vortex phase. We observed twofold symmetric in-plane resistance due to the unique motion of liquid crystal vortices. Moreover, the suppression of resistance in the field H_{kink} at which the kink appears is caused by the pinning of the three-dimensional (3D) vortex. The anomaly of the resistance at high temperatures may be a CDW transition or a freezing of random Fe spins.

II. EXPERIMENT

Single crystals of Fe_xNbS_2 were grown by the chemical vapor transport method. We used a mixture of Nb (99.9%, Kojundo Chem.) and S (99.99%, Kojundo Chem.) powders. Fe powder (99.9%, Kojundo Chem.) was added to the mixture in a stoichiometric ratio of 0.08% Fe. We do not encapsulate iodine in the quartz tube as a transport agent. A quartz tube in which the mixture was vacuum sealed was placed in a furnace at 900 °C for three weeks. The furnace was heated at 10 °C/min until it reached a temperature of 900 °C. The temperature gradient was 3 °C/cm. When removing the quartz tube from the furnace, we quench the hot side of the quartz tube with liquid nitrogen.

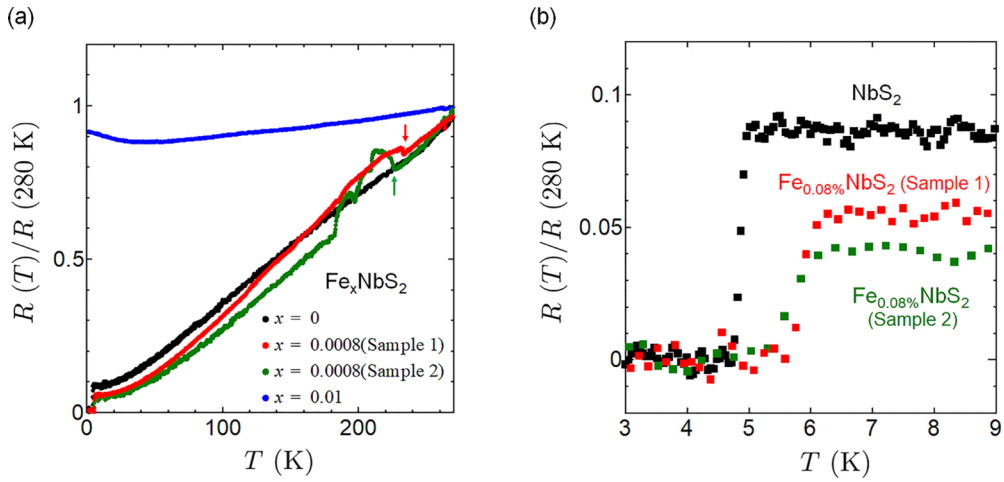

FIG. 1. Electric transport properties in Fe_xNbS_2. (a) Temperature dependence of normalized resistance $R(T)/R(280\,\mathrm{K})$ for pure ($x = 0$), $Fe_{0.08\%}NbS_2$, and $Fe_{1\%}NbS_2$. (b) Enlargement of the dependence of normalized resistance $R(T)/R(280\,\mathrm{K})$ on temperature around T_c for NbS_2 and $Fe_{0.08\%}NbS_2$.

We determined the lattice constants and polytypes for single crystals by using x-ray diffraction measurements. The lattice constant of $Fe_{0.08\%}NbS_2$ and pure NbS_2 are shown in Table 1 of the Supplemental Material [19]. The x-ray results show that our samples have a 2H polytype structure. We found that $Fe_{0.08\%}NbS_2$ can distinguish the a axis from the b axis by measuring the angle of the corners of the single crystal; see the Supplemental Material, Fig. S1 [19]. We confirmed that the Fe concentration of the synthesized sample is 0.08% $\pm$ 0.03% from the magnetic susceptibility results using the

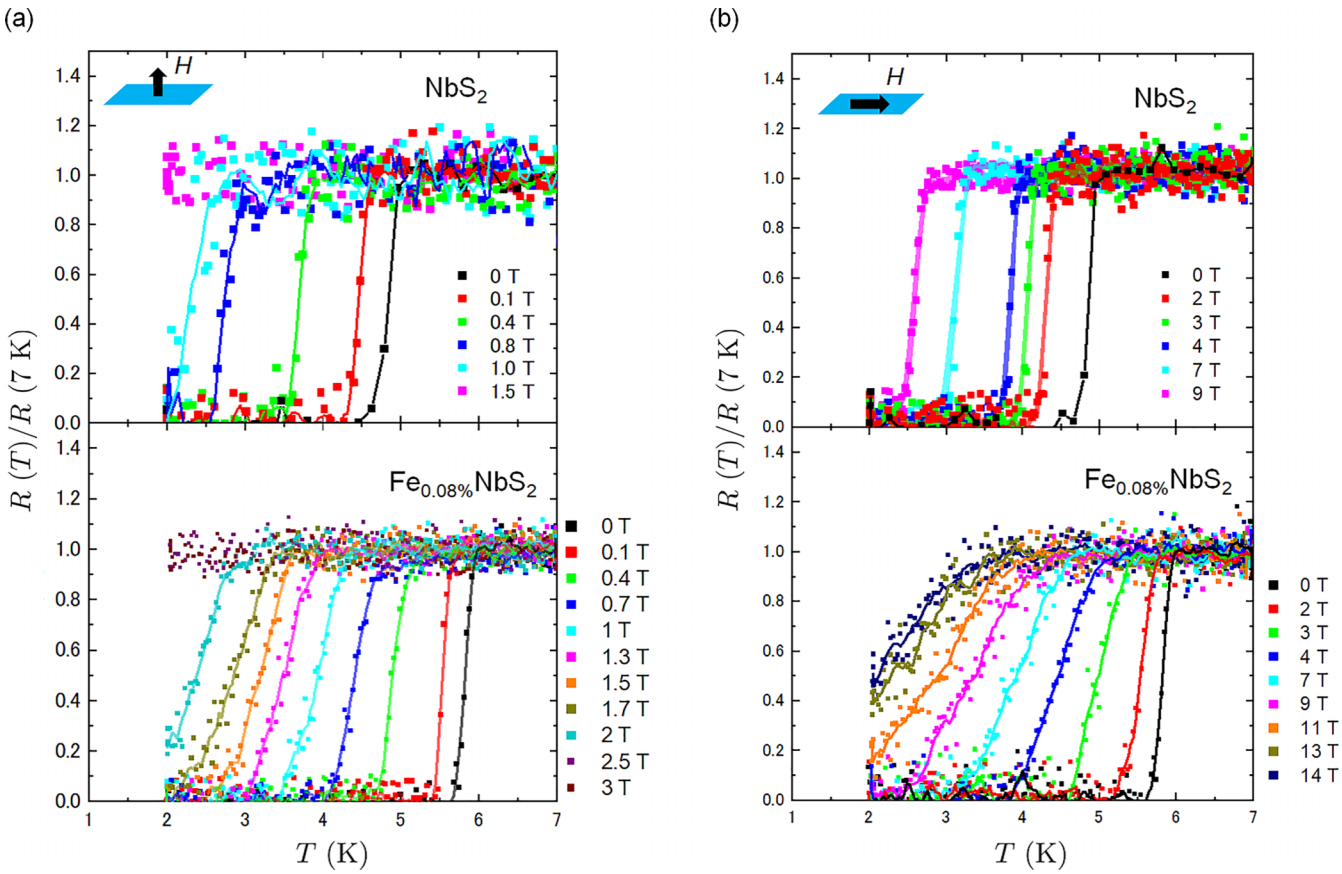

FIG. 2. Temperature dependence of resistance for (a) out-of-plane magnetic fields $H_\perp$ and (b) in-plane magnetic fields $H_\parallel$ for NbS_2 and $Fe_{0.08\%}NbS_2$. Each resistance is normalized by the normal resistance at 7 K.

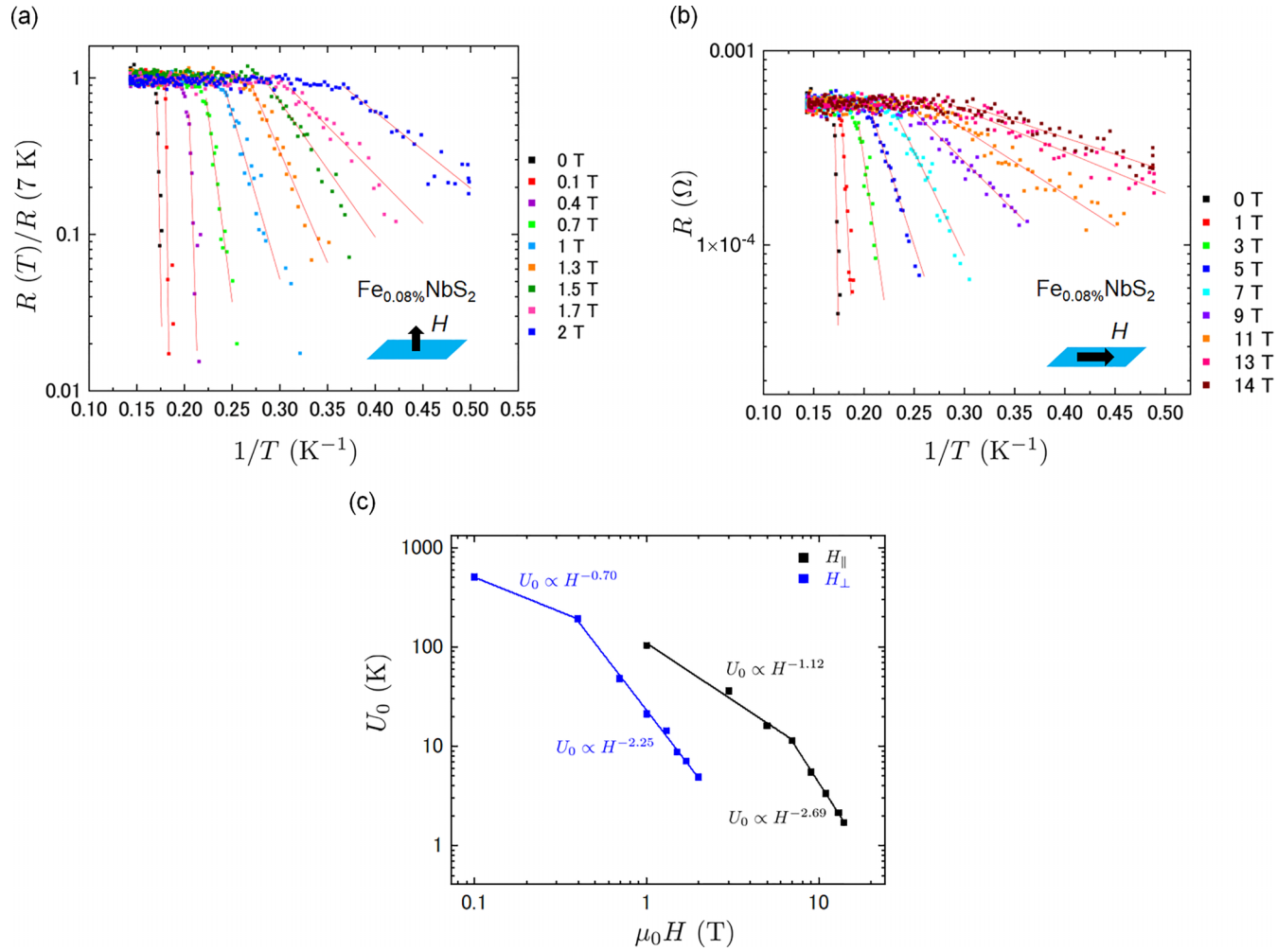

FIG. 3. Thermally activated vortex flow. (a),(b) Arrhenius plot of the resistance in $Fe_{0.08\%}NbS_2$ for $H_\perp$ and $H_\parallel$, respectively. (c) Magnetic field dependence of the activation energy U_0 for both field orientations. The lines represent power-law fits.

magnetic property measurement system (MPMS) (Quantum Design). The result is shown in the Supplemental Material, Fig. S2 [19].

In the DC measurements, a bias current of ±100 μA was applied by a DC source (6220, Keithley) and the voltage was measured with a nanovoltmeter (34420A, Keysight). Voltage terminals were attached to the conducting plane using gold wires with a diameter of 20 μm. The bias current was applied in parallel to the a axis. The bias current is sufficiently less than the critical current for our samples, as shown in the Supplemental Material, Fig. S3 [19]. The measured single crystals were typically about $1 \times 0.8 \times 0.2$ mm. The electrical resistance was measured by the four-terminal method using the Physical Property Measurement System (PPMS) (Quantum Design) with a horizontal rotator probe at T down to 2 K with magnetic fields of up to 14 T.

III. RESULTS AND DISCUSSION

Figure 1(a) shows the temperature dependence of the normalized resistance at 280 K for Fe_xNbS_2 ($x = 0$, 0.0008, 0.01). The superconducting transition temperature of pure NbS_2 is 4.9 K, which is consistent with previous reports [15,20]. On the other hand, $Fe_{0.08\%}NbS_2$ samples show a resistance anomaly at 226 and 233 K, respectively, as shown in Fig. 1(a). This anomaly was not observed in pure NbS_2 or $Fe_{1\%}NbS_2$. $Fe_{0.08\%}NbS_2$ exhibited a superconducting transition at ~ 6.1 K. In general, a magnetic impurity suppresses superconductivity, but the T_c of the $Fe_{0.08\%}$ samples is higher than that of pure NbS_2 [Fig. 1(a)]. In our previous report [17], we observed that in samples doped with 1% Fe, the resistance behavior at low temperatures exhibited the Kondo effect without superconductivity.

In contrast to other MX_2 materials such as 2H-$NbSe_2$, 2H-$TaSe_2$, and 2H-TaS_2, 2H-NbS_2 does not exhibit CDW and is known to be superconductive. However, the anomaly of the resistance at high temperatures, as shown in Fig. 1(b), is similar to the behavior of the CDW transition in 2H-MX_2 [14]. Recently, exciting results have been reported on the presence of CDW order in 2H-NbS_2. For example, satellite peaks due to $\sqrt{13} \times \sqrt{13}$ CDW have been observed at 77 K in pure NbS_2 using diffuse x-ray scattering measurements [21]. They suggest that bulk 2H-NbS_2 contain dilute 1T layers because 1T-MX_2 materials exhibit the feature of $\sqrt{13} \times \sqrt{13}$ CDW. An STM study has revealed the presence of an incommensurate CDW at 4.5 K pinned by atomic impurities [22]. Our

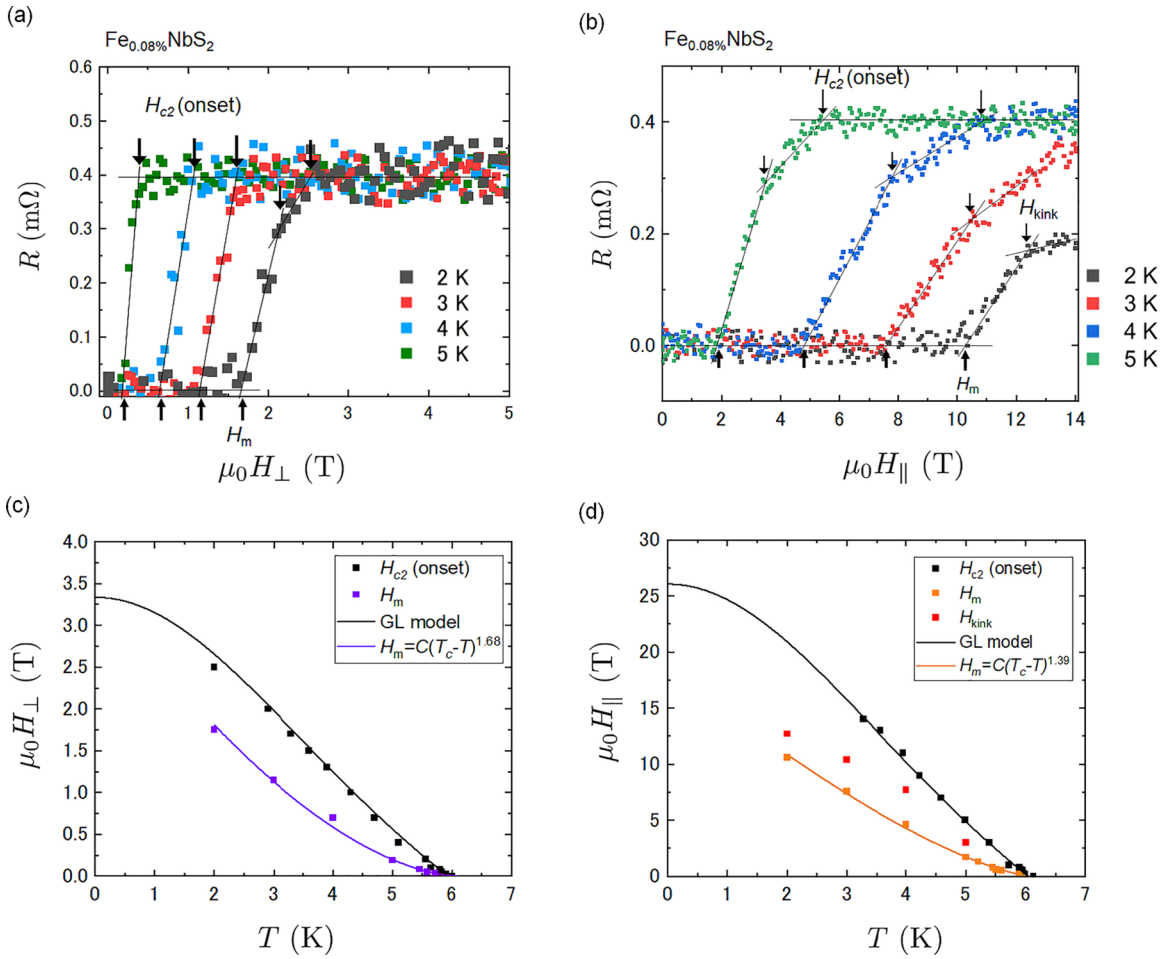

FIG. 4. Vortex solid-liquid transition. (a),(b) Magnetic field dependence of resistance for $H_\perp$ and $H_\parallel$ in $Fe_{0.08\%}NbS_2$. (c),(d) $H-T$ phase diagrams for $H_\perp$ and $H_\parallel$, respectively. The dotted lines show the results that fit with the 3D GL model. Solid lines represent the fitting results with the melting curve expressed by $H_m = C(T_c - T)^a$.

result of the resistivity anomaly at high temperatures suggests the possibility of a CDW transition in the 2H structure based on the x-ray results. Another possibility is that random Fe spin freezing is causing the resistance anomaly. The superconducting properties of $Fe_{0.08\%}NbS_2$ are described in detail below.

Figure 2 shows the dependence of resistance on temperature as a magnetic field was applied in-plane $H_\parallel$ and out-of-plane $H_\perp$ for pure and $Fe_{0.08\%}NbS_2$. The pure NbS_2 shows a sharp superconducting transition. On the other hand, the transition width in $Fe_{0.08\%}NbS_2$ is broader than that in the pure NbS_2. The broadening of the resistive transitions for the applied magnetic field is caused by a vortex flow in type-II superconductors [23]. This has been reported in various superconductors [24–26]. Here we analyze the contribution of a thermally activated vortex flow. The behavior of the vortex flow is well described as

$$R(T,H) = R_0 \exp\left(-\frac{U(T,H)}{k_B T}\right), \tag{1}$$

where $U(T,H)$ is the activation energy for vortex hopping and k_B is Boltzmann's constant, and we assume $U(T,H) = U_0(H)(1 - T/T_c)$. This pinning potential U_0 can be obtained from the slope of Arrhenius plots, as shown in Figs. 3(a) and 3(b). The red lines show the results of linear fitting. We have plotted the magnetic field dependence of the activation energy U_0 for $H_\perp$ and $H_\parallel$ in Fig. 3(c). The results show a power-law dependence on the magnetic field, $U_0(H) \propto H^{-\alpha}$ with $\alpha \sim 0.70$ for $H_\perp < 0.4\,\mathrm{T}$, $\alpha \sim 2.25$ for $H_\perp > 0.4\,\mathrm{T}$, and $\alpha \sim 1.12$ for $H_\parallel < 7\,\mathrm{T}$, $\alpha \sim 2.69$ for $H_\parallel > 7\,\mathrm{T}$. Similar behavior has been reported in previous reports [24,27]. The difference between the U_0 values of $H_\perp$ and $H_\parallel$ indicates that the vortex flow is anisotropic. Our previous findings [17] indicate that Fe atoms primarily enter the interlayer. As a result, pinning has a more substantial effect on vortex flow in the in-plane field than in the out-of-plane field. When the applied magnetic field increases, the Lorentz force for the vortex exceeds the pinning force. The crossover between the Lorentz and pinning forces occurs when the interactions between vortex bundles become significant, known as collective pinning [28].

Figures 4(a) and 4(b), respectively, show magnetoresistance data for $H_\perp$ and $H_\parallel$ in $Fe_{0.08\%}NbS_2$. A kink clearly appears when the magnetic field is applied parallel to the plane. The kink was also observed for $H_\perp$ at 2 K. This behavior is reproduced in other samples (see the Supplemental Material, Fig. S5(a) [19]). The obtained $H-T$ phase diagram is shown in Figs. 4(c) and 4(d). Here, T_c for various magnetic fields is identified as the onset temperature. The melting field

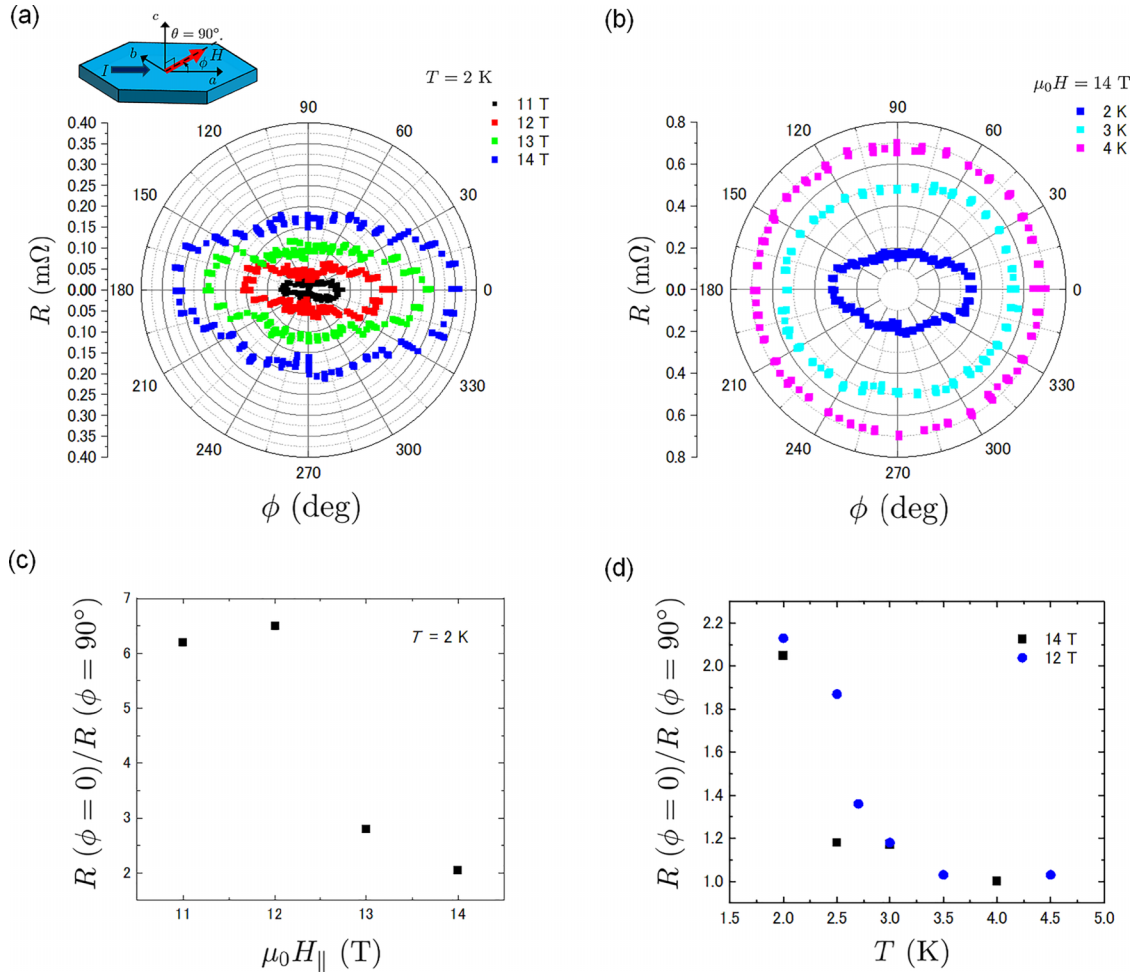

FIG. 5. The ϕ dependence of vortex flow for in-plane magnetic fields. (a) Angular dependence of magnetoresistance for $Fe_{0.08\%}NbS_2$ at 2 K. (b) Temperature dependence of the magnetoresistance at 14 T. (c) $R(\phi = 0)/R(\phi = 90°)$ for magnetic fields at 2 K. (d) $R(\phi = 0)/R(\phi = 90°)$ for various temperatures for 12 and 14 T.

at which the finite resistance appears is represented as H_m, and the field at which the kink structure appears is denoted as H_{kink}. The T_c and H_{c2} of $Fe_{0.08\%}NbS_2$ shift to a higher temperature and field than those of pure NbS_2, as shown in the Supplemental Material, Fig. S4 [19]. This means that the superconductivity of $Fe_{0.08\%}NbS_2$ is more robust against applied magnetic fields. In the framework of the Bardeen-Cooper-Schrieffer (BCS) theory, the Pauli paramagnetic limit is described as $H_P = \Delta/\sqrt{2}\mu_B = 1.84T_c$, where Δ is the superconducting gap and μ_B is the Bohr magneton. By substituting $T_c = 6.1$ K for $Fe_{0.08\%}NbS_2$, $\mu_0 H_P$ is estimated to be 11.2 T. We note that $\mu_0 H_P$ for pure NbS_2 with a T_c of 5 K is estimated to be 9.2 T. We found superconductivity beyond the Pauli limit in $Fe_{0.08\%}NbS_2$. A small amount of Fe impurities enhances the superconductivity. Here, we discuss the relationship between H_{c2} and T_c based on the anisotropic Ginzburg-Landau (GL) model, assuming that H_{c2} is determined by the orbital effect. The anisotropic GL model [29] is given by Eqs. (2) and (3),

$$\mu_0 H_{c2\perp}(T) = \frac{\Phi_0}{2\pi\xi_{ab}(0)^2}(1 - T/T_c), \tag{2}$$

for the out-of-plane $H_{c2\perp}$, and

$$\mu_0 H_{c2\parallel}(T) = \frac{\Phi_0}{2\pi\xi_{ab}(0)\xi_c(0)}(1 - T/T_c), \tag{3}$$

for the in-plane $H_{c2\parallel}$, where μ_0 is the vacuum permeability and Φ_0 is the magnetic flux quantum. The upper critical field determined by the orbital effect at $T = 0$ is given by [30]

$$\mu_0 H_{c2}(0) = -0.69T_c\left(\frac{\mu_0 dH_{c2}}{dT}\right)_{T=T_c}, \tag{4}$$

where $\mu_0 dH_{c2}/dT$ is the initial slope at T_c. We determined $H_{c2\perp}(0) \sim 3.3$ T and $H_{c2\parallel}(0) \sim 26$ T using initial slope values of $\frac{\mu_0 dH_{c2}}{dT} \sim -0.78$ and -6.14, respectively. The solid lines in Figs. 4(c) and 4(d) show the fitting result. We obtained the in-plane coherence length $\xi_{ab}(0) \sim 99$ Å and the out-of plane coherence length $\xi_c(0) \sim 12$ Å for $Fe_{0.08\%}NbS_2$. $\xi_c(0) \sim 12$ Å is twice the layer spacing of 6 Å for 2H-NbS_2.

The $H_m - T$ plot curves upwards toward low temperatures. In cuprate superconductors, it is known that the temperature dependence of H_m is related to $H_m \propto (T_c - T)^a$, where a is a critical exponent. This means a transition from a vortex solid

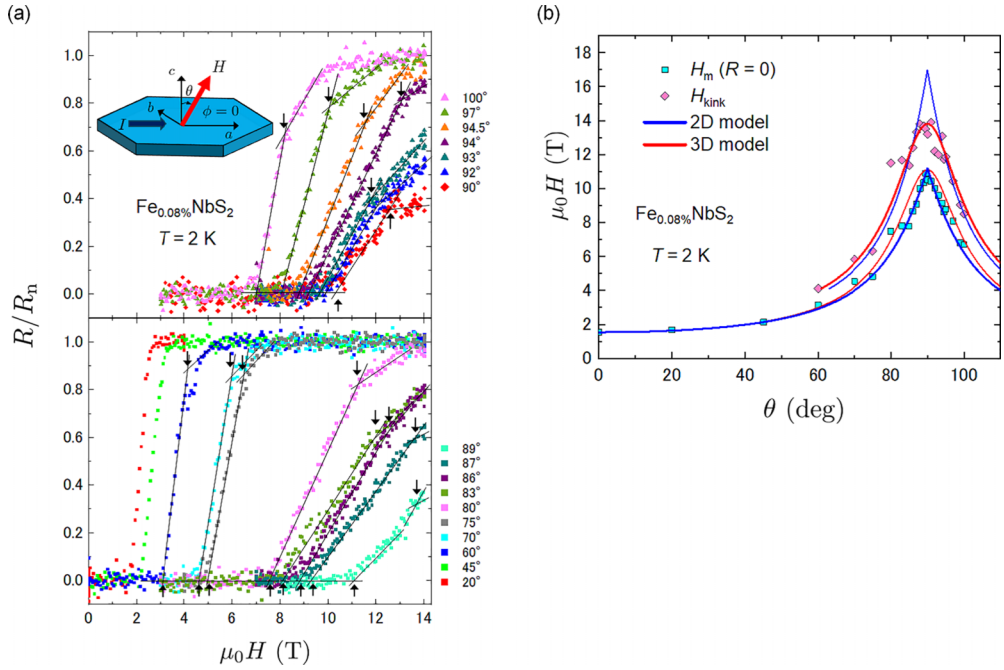

FIG. 6. The θ dependence of vortex flow. (a) Angular dependence of magnetoresistance for $Fe_{0.08\%}NbS_2$ at 2 K. (b) Angular dependence of the upper critical field at 2 K for H_m ($R = 0$) and H_{kink}. The blue and red solid lines are fitted by the 2D Tinkham and the anisotropic 3D models, respectively.

(glass) to a liquid. We have found a good fit with $a = 1.68$ for $H_\perp$ and $a = 1.39$ for $H_\parallel$, as shown in Figs. 4(c) and 4(d). In particular, the behavior at $a = 1.4$ has been reported to be a smectic solid-liquid transition [12]. Therefore, our result for $H_\parallel$ suggests the realization of a smectic vortex phase.

To reveal the liquid crystal vortex in more detail, we investigated the angular dependence of magnetoresistance under in-plane and out-of-plane directions. Figure 5(a) shows the angular dependence of magnetoresistance at 2 K for in-plane magnetic fields. ϕ is defined as the angle between the a axis and the applied magnetic field, as shown in Fig. 5(a). Our observation revealed a twofold modulation of the magnetoresistance. Specifically, the magnetoresistance shows a maximum value when the magnetic field ($\phi = 0°, 180°$) is applied parallel to the bias current along the a axis (see the Supplemental Material, Fig. S5(b) [19]). The motion of the Josephson vortex between the layers cannot explain this result. This is because, at $H \parallel I$, the Lorentz force does not act on the Josephson vortex. The magnetic field dependence and temperature dependence of the $R(\phi = 0)/R(\phi = 90°)$ values are plotted in Figs. 5(c) and 5(d), respectively. At 2 K, the $R(\phi = 0)/R(\phi = 90°)$ value is suppressed above 12 T. This magnetic field of 12 T is close to that of H_{kink} in Fig. 4(b). In other words, the range of the magnetic field, $H_m < H < H_{kink}$, shows a larger twofold symmetric in-plane anisotropy. This refers to a change from a smectic phase to a different liquid crystal vortex phase, such as nematic. Intriguingly, the twofold modulation is observed in the superconducting state, as shown in Fig. 5(d).

Figure 6(a) shows the angular dependence of the magnetoresistance with various θ angles ($\phi = 0$) at 2 K for $Fe_{0.08\%}NbS_2$. Here, θ represents the angle between the c axis and the applied magnetic field, as shown in Fig. 6(a). When the angle reaches 90 degrees, the resistive transition from $R = 0$ (vortex lattice melting) shifts to the highest field side. We observed a kinked structure in the broad resistive transition, as shown by the black arrows in Fig. 6(a). This structure is most pronounced around 90 degrees. Figure 6(b) shows the angular dependence of the vortex melting field $H_m(R = 0)$ and H_{kink}, respectively. There are two possible models for the angular dependence of H_{c2} for layered superconductors. The first is the 3D anisotropic GL model [29], which can be expressed as

$$\left(\frac{H_{c2}(\theta)\cos\theta}{H_{c2\perp}}\right)^2 + \left(\frac{H_{c2}(\theta)\sin\theta}{H_{c2\parallel}}\right)^2 = 1. \tag{5}$$

The other is the 2D Tinkham model, which takes account of the Josephson coupling between superconducting layers [31]. The equation is given by

$$\left|\frac{H_{c2}(\theta)\cos\theta}{H_{c2\perp}}\right| + \left(\frac{H_{c2}(\theta)\sin\theta}{H_{c2\parallel}}\right)^2 = 1. \tag{6}$$

Using these models, we performed a fitting analysis for the angular dependence of H_m and H_{kink}. The results are shown as red and blue solid lines in Fig. 6(b). Interestingly, for $H_m - \theta$, the blue line in the 2D Tinkham model fits better than the red line fitted by the 3D model at around 90 degrees. This implies that two-dimensional superconductivity is realized in a low field near 90 degrees. On the other hand, the $H_{kink} - \theta$ result can be explained by the red line in the 3D anisotropic GL model. In other words, there is a crossover from 2D to 3D superconducting behavior at low temperatures for $H_\parallel$. We note that the angular dependence of H_m in Fig. 6(b) is symmetric around 90 degrees, while that of the H_{kink} values shows slight data variability. This may be due to the vortex liquid

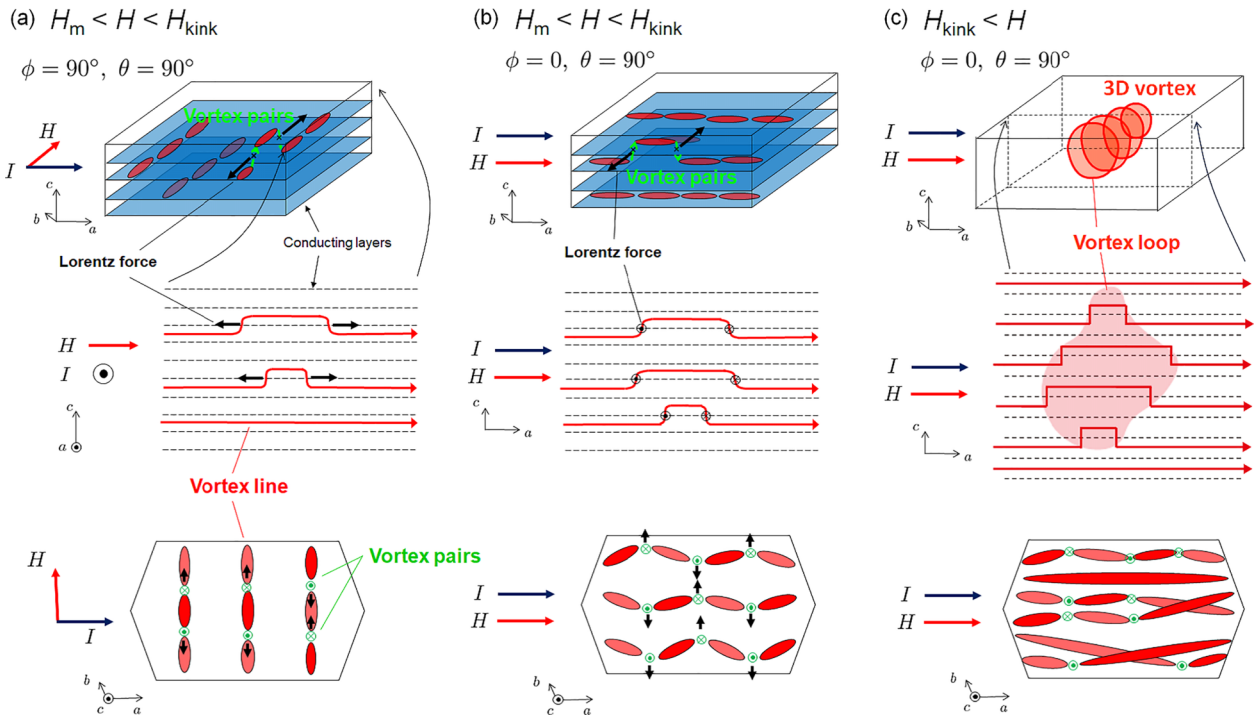

FIG. 7. Schematic of liquid crystal vortices. Vortex lines hopping to adjacent layers create vortex pairs. (a) For $H_m < H < H_{\rm kink}$, thermally excited vortex pairs in the conducting plane move due to the Lorentz force, resulting in finite resistance. When the magnetic field H is perpendicular to the current I, sliding allows the vortex pair to move to neighboring interlayers. (b) In $H \parallel I$, vortex pairs are stable due to the inability of Lorentz forces to eliminate them. Greater vortex flow resistance occurs than in situation (a). (c) In $H_{\rm kink} < H$, vortex pairs in the conducting plane are pinned by forming a vortex loop (middle). The alignment of vortex loops results in a three-dimensional vortex, making it difficult for vortex pairs in the conduction plane to move.

state above $H > H_m$. The difference in pinning is affected by random Fe atoms entering the interlayers (see the Supplemental Material, Fig. S6 [19]).

Below, we discuss the origin of the twofold symmetric in-plane anisotropy and the kink structure in the magnetoresistance data. Generally, when a vortex flow occurs, the resistance increases because of dissipation. We consider the detection of the vortex flow in the conducting plane based on the arrangement of voltage terminals and the result in Fig. 6(b). A vortex pair is generated in the conducting plane by hopping of the vortex line between interlayers by thermal excitation, as shown in Fig. 7. The Lorentz force acting on the vortex pair remains unchanged, regardless of the direction of the in-plane magnetic field, as depicted in Figs. 7(a) and 7(b). In the configuration of $H \perp I$, in Fig. 7(a), the vortex pair can be removed through sliding, driven by the Lorentz force. This means that the vortex line shifts to the neighboring interlayer. On the other hand, in $H \parallel I$, the vortex pair exists stably in the conducting layer, which cannot be eliminated by sliding [Fig. 7(b)]. More vortex pairs are present in conduction planes. Therefore, the twofold symmetry observed in the in-plane resistance results from the difference in the number of vortex pairs.

The resistance above $H_{\rm kink}$ is suppressed and appears as the kink structure. Based on the results presented in Fig. 6, the 2D vortex flow state changes to a 3D vortex pinning. Vortex pairs in the interlayer direction form vortex loops as drawn in the middle of Fig. 7(c). Furthermore, the aligned vortex loops form a three-dimensional vortex. The 3D vortex solid is responsible for the appearance of the kink structure. Under high magnetic fields above $H_{\rm kink}$, there may be a transition from the smectic to a nematic phase [7,32].

The two-dimensionality enhances the H_{c2} and T_c in layered Fe-doped NbS_2 superconductors. In the future, we can further develop our research on liquid-crystal-like vortex phases and the relationship between the superconductivity and the Kondo effect or spin glass in MX_2 materials. It is possible to prove the presence of the quantum Hall effect in the smectic vortex liquid state of MX_2 systems.

IV. CONCLUSION

In conclusion, we have investigated the electric transport properties in layered dilute Fe-doped NbS_2 superconductors. We observed a resistance anomaly at high temperatures, which is not found in pure NbS_2. $Fe_{0.08\%}NbS_2$ exhibited a resistive transition caused by the vortex motion. The magnetic field dependence of the pinning potential U_0 exhibits power-law behavior. From the temperature and angular dependence of H_m, we observed the liquid crystal phase due to vortices confined in the interlayers. The twofold-symmetric resistance for the in-plane is due to the different number of vortex pairs stably present on the conduction plane, as the liquid crystalline vortex lines hop between adjacent layers. At higher magnetic fields, the 3D vortices are pinned, resulting in the appearance of the kink structure. Our findings for MX_2 materials will contribute to the development of quantum

liquid-crystal-like vortex physics in two-dimensional boson systems.

ACKNOWLEDGMENTS

We thank K. Onodera, K. Isono, R. Ogata, T. Kurosawa, K. Ichimura, N. Matsunaga, and K. Nomura for their experimental help and valuable discussions. This work was supported by Nippon Sheet Glass Foundation for Material Science and Engineering, Yashima Environment Technology Foundation, Inamori Foundation, Iketani Science and Technology Foundation, and Samco Science and Technology Foundation.

[1] P. M. Chaikin and T. C. Lubensky, *Principles of Condensed Matter Physics* (Cambridge University Press, Cambridge, 1995).
[2] G. E. Volovik, *The Universe in a Helium Droplet* (Oxford University Press, Oxford, 2003).
[3] V. L. Berezinskii, Sov. Phys. JETP **34**, 610 (1972).
[4] J. M. Kosterlitz and D. J. Thouless, J. Phys. C **6**, 1181 (1973).
[5] L. Balents and D. R. Nelson, Phys. Rev. B **52**, 12951 (1995).
[6] D. R. Nelson and H. S. Seung, Phys. Rev. B **39**, 9153 (1989).
[7] E. W. Carlson, A. H. Castro Neto, and D. K. Campbell, Phys. Rev. Lett. **90**, 087001 (2003).
[8] J. Kierfeld, T. Nattermann, and T. Hwa, Phys. Rev. B **55**, 626 (1997).
[9] B. Horovitz, Phys. Rev. B **51**, 3989 (1995).
[10] G. Blatter, M. V. Feigel'man, V. B. Geshkenbein, A. I. Larkin, and V. M. Vinokur, Rev. Mod. Phys. **66**, 1125 (1994).
[11] S. N. Gordeev, A. A. Zhukov, P. A. J. de Groot, A. G. M. Jansen, R. Gagnon, and L. Taillefer, Phys. Rev. Lett. **85**, 4594 (2000).
[12] S. A. Baily, B. Maiorov, H. Zhou, F. F. Balakirev, M. Jaime, S. R. Foltyn, and L. Civale, Phys. Rev. Lett. **100**, 027004 (2008).
[13] X. Liu, Y. X. Chong, R. Sharma, and J. S. Davis, Science **372**, 1447 (2021).
[14] M. Naito and S. Tanaka, J. Phys. Soc. Jpn. **51**, 219 (1982).
[15] C.-w. Cho, J. Lyu, C. Y. Ng, J. J. He, K. T. Lo, D. Chareev, T. A. Abdel-Baset, M. Abdel-Hafiez, and R. Lortz, Nat. Commun. **12**, 3676 (2021).
[16] A. H. Castro Neto, Phys. Rev. Lett. **86**, 4382 (2001).
[17] H. Nobukane, Y. Tabata, T. Kurosawa, D. Sakabe, and S. Tanda, J. Phys.: Condens. Matter **32**, 165803 (2020).
[18] S. Park, V. Barrena, S. Mañas-Valero, J. J. Baldoví, A. Fente, E. Herrera, F. Mompeán, M. García-Hernández, Á. Rubio, E. Coronado *et al.*, Nat. Commun. **12**, 4668 (2021).
[19] See Supplemental Material at http://link.aps.org/supplemental/10.1103/PhysRevB.109.174505 for x-ray diffraction measurements, the temperature dependence of susceptibility, the current-voltage characteristics, the $H-T$ phase diagram, the result for sample 2, and the comparison of magnetoresistance.
[20] K. Onabe, M. Naito, and S. Tanaka, J. Phys. Soc. Jpn. **45**, 50 (1978).
[21] M. Leroux, L. Cario, A. Bosak, and P. Rodière, Phys. Rev. B **97**, 195140 (2018).
[22] C. Wen, Y. Xie, Y. Wu, S. Shen, P. Kong, H. Lian, J. Li, H. Xing, and S. Yan, Phys. Rev. B **101**, 241404(R) (2020).
[23] M. Tinkham, Phys. Rev. Lett. **61**, 1658 (1988).
[24] T. T. M. Palstra, B. Batlogg, R. B. van Dover, L. F. Schneemeyer, and J. V. Waszczak, Phys. Rev. B **41**, 6621 (1990).
[25] C. Tarantini, A. Gurevich, J. Jaroszynski, F. Balakirev, E. Bellingeri, I. Pallecchi, C. Ferdeghini, B. Shen, H. H. Wen, and D. C. Larbalestier, Phys. Rev. B **84**, 184522 (2011).
[26] H. Nobukane, K. Yanagihara, Y. Kunisada, Y. Ogasawara, K. Isono, K. Nomura, K. Tanahashi, T. Nomura, T. Akiyama, and S. Tanda, Sci. Rep. **10**, 3462 (2020).
[27] B. Y. Wang, D. Li, B. H. Goodge, K. Lee, M. Osada, S. P. Harvey, L. F. Kourkoutis, M. R. Beasley, and H. Y. Hwang, Nat. Phys. **17**, 473 (2021).
[28] A. I. Larkin and Y. N. Ovchinnikov, J. Low Temp. Phys. **34**, 409 (1979).
[29] W. E. Lawrence and S. Doniach, in *Proceedings of the 12th International Conference on Low Temperature Physics*, edited by E. Kanda (Academic Press, Kyoto, 1971), p. 361.
[30] N. R. Werthamer, E. Helfand, and P. C. Hohenberg, Phys. Rev. **147**, 295 (1966).
[31] M. Tinkham, Phys. Rev. **129**, 2413 (1963).
[32] S. A. Kivelson, E. Fradkin, and V. J. Emery, Nature (London) **393**, 550 (1998).